Documenting Storm Severity in the Mid-Atlantic Region Using Lightning and Radar Information

SCOTT D. RUDLOSKY* AND HENRY E. FUELBERG

Department of Earth, Ocean, and Atmospheric Science, The Florida State University, Tallahassee, Florida

(Manuscript received 2 October 2012, in final form 17 January 2013)

ABSTRACT

Storm severity in the mid-Atlantic region of the United States is examined using lightning, radar, and model-derived information. Automated Warning Decision Support System (WDSS) procedures are developed to create grids of lightning and radar parameters, cluster individual storm features, and data mine the lightning and radar attributes of 1252 severe and nonsevere storms. The study first examines the influence of serial correlation and uses autocorrelation functions to document the persistence of lightning and radar parameters. Decorrelation times are found to vary by parameter, storm severity, and mathematical operator, but the great majority are between three and six lags, suggesting that consecutive 2-min storm samples (following a storm) are effectively independent after only 6–12 min. The study next describes the distribution of lightning jumps in severe and nonsevere storms, differences between various types of severe storms (e.g., severe wind only), and relationships between lightning and radar parameters. The 2σ lightning jump algorithm (with a 10 flashes min^{-1} activation threshold) yields 0.92 jumps h^{-1} for nonsevere storms and 1.44 jumps h^{-1} in severe storms. Applying a 10-mm maximum expected size of hail (MESH) threshold to the 2σ lightning jump algorithm reduces the frequency of lightning jumps in nonsevere storms to 0.61 jumps h^{-1}. Although radar-derived parameters are comparable between storms that produce severe wind plus hail and those that produce tornadoes, tornadic storms exhibit much greater intracloud (IC) and cloud-to-ground (CG) flash rates. Correlations further illustrate that lightning data provide complementary storm-scale information to radar-derived measures of storm intensity.

1. Introduction

Advances in lightning datasets and storm analysis techniques are improving our understanding of relationships between storm-scale processes and lightning production. The emergence and expansion of total lightning datasets hold great promise for researchers and operational forecasters. Darden et al. (2010) found that incorporating real-time total lightning data into severe weather forecasting procedures improved warning confidence, and suggested potential improvement in short-term warning lead times. However, they also noted the limited use of lightning information in the National Weather Service (NWS) convective warning program. They suggested that this was due to the lack of total lightning information at regional and national scales, limited knowledge about relationships between lightning and severe weather, and a cultural legacy of perceiving lightning data as less important than traditional radar and satellite products.

Many studies have shown that sudden increases in intracloud (IC) lightning flash rate, colloquially known as lightning jumps, often precede severe weather occurrence[1] (e.g., Goodman et al. 1988; MacGorman et al. 1989; Williams et al. 1989, 1999; Buechler et al. 2000; Lang et al. 2000; Goodman et al. 2005; Wiens et al. 2005; Tessendorf et al. 2007; Steiger et al. 2007; Gatlin and Goodman 2010; Darden et al. 2010; Schultz et al. 2009, 2011). The lightning jump signature is a useful proxy for identifying strengthening updrafts and increasing storm

* Current affiliation: NOAA/Center for Satellite Applications and Research, College Park, Maryland.

Corresponding author address: Scott D. Rudlosky, ESSIC/CICS, University of Maryland, College Park, 5825 University Research Court, Suite 4001, College Park, MD 20740-3823.
E-mail: scott.rudlosky@noaa.gov

[1] As presently defined by the U.S. NWS, that is, thunderstorms with at least one tornado, hail ≥1 in. (2.54 cm), and/or winds ≥ 58 mi h^{-1} (93.3 km h^{-1}).

DOI: 10.1175/MWR-D-12-00287.1

intensity and helps forecasters to identify storms acquiring severe potential and determine where a storm is in its life cycle (Darden et al. 2010). Lightning jumps also have been observed prior to severe hail and wind. For example, Goodman et al. (2005) examined a severe pulse thunderstorm that exhibited a strong increase in IC flash rate 9 min before damaging winds occurred at the surface. Gatlin and Goodman (2010) and Schultz et al. (2009, 2011) have quantified this relationship to develop lightning jump algorithms that provide an early indication (warning) of severe weather. Using lightning data alone, the algorithm described by Schultz et al. (2011) predicted severe weather with a 20.65-min lead time, a 79% probability of detection (POD), and a 36% false alarm rate (FAR).

The National Lightning Detection Network (NLDN; Orville 2008) has provided cloud-to-ground (CG) lightning data to NWS forecasters for over a decade, and a select few NWS offices also receive IC data from local Lightning Detection and Ranging (LDAR; Boccippio et al. 2001) and Lightning Mapping Array (LMA; Rison et al. 1999) networks. The Washington, D.C., Lightning Mapping Array (DCLMA; Krehbiel 2008) is a joint demonstration project between the National Aeronautics and Space Administration (NASA), National Oceanic and Atmospheric Administration (NOAA), New Mexico Institute of Mining and Technology, and 10 local site hosts. The DCLMA has been operational since 2007, providing detailed 3D lightning observations that inform decision makers about severe weather and lightning threats. The network consists of 10 sensors that monitor very high frequency (VHF; MHz) radio waves (radiation sources) emitted by lightning. Since IC discharges radiate mainly in the VHF range (Betz et al. 2004) and VHF radio waves travel along a line of sight, the DCLMA is most sensitive to IC flashes and the upper portions of CG flashes (Thomas et al. 2001). Conversely, the NLDN is most sensitive to low (very low) frequency [LF (VLF); kHz] emissions from CG return strokes, which radiate mainly in this range (Betz et al. 2004). The combination of DCLMA and NLDN observations provides detailed insights into the structure and evolution of lightning activity in the mid-Atlantic region.

Forecasters will continue to rely on traditional methods (e.g., radar and satellite) for monitoring thunderstorms despite improving lightning detection technologies and the development of lightning jump algorithms (Schultz et al. 2009). Therefore, it is important to determine the degree to which lightning data complement the more traditional radar-derived measures of storm intensity. Updraft trends are especially useful in assessing storm severity (MacGorman et al. 2008), but can be difficult to obtain from radar in real time (Weber et al. 1998; MacGorman et al. 2008). NWS forecasters currently use individual plan position indicator (PPI) slices to monitor rapidly evolving storms, but some storms remain under sampled, especially those distant from the radar, because of radar latency and beam geometry. Several studies have shown that dual-polarization signatures (e.g., ZDR) are helpful for discerning updraft intensification (Illingworth et al. 1987; Loney et al. 2002; Romine et al. 2008), and the nationwide upgrade to dual-polarization technology (Ryzhkov et al. 2005) will increase the use of these data in operations. Nonetheless, radars require time to scan volumes while LMA networks provide continuous 3D lightning information. Much like the rapid sampling provided by phased array radar (Heinselman et al. 2008; Heinselman and Torres 2011; Bluestein et al. 2010), knowledge of rapidly changing lightning patterns might increase warning confidence by augmenting existing and future radar and satellite products.

The immensity of lightning and radar datasets, together with somewhat limited software capabilities, has restricted the scope of many previous studies. However, the Warning Decision Support System–Integrated Information (WDSS-II; Lakshmanan et al. 2007) and geographic information system (GIS) software now provide an ideal framework for developing large lightning and radar datasets and determining relationships between them. Automated WDSS-II procedures have been developed to create grids of lightning and radar parameters, cluster individual storm features, and data mine lightning and radar attributes from severe and nonsevere storms. These procedures allow streamlined database development and analysis, help minimize the manual inspection of storm features while maximizing accuracy, and facilitate detailed analysis of lightning and radar parameters in many severe and nonsevere storms.

This study focuses on the mid-Atlantic region of the United States where varying terrain and lifting mechanisms determine both the timing (seasonal and diurnal) and type (wind, hail, and tornado) of severe weather. The region experiences a mix of convective modes (e.g., discrete supercells, isolated pulse storms, forward-propagating multicell structures, and bowing line segments). Mesoscale influences on storm development are strongly controlled by variations in the underlying surface. Terrain in the study area varies from mountains in the west (elevations of 600–1200 m) to coastal plains, bodies of water, and complex coastlines in the east (Fig. 1a). Orographic thermal forcing dominates western (mountainous) portions of the study domain, while the sea breeze strongly influences convection in the coastal regions.

The goal of this study is to combine information about the near-storm environment, radar-defined storm

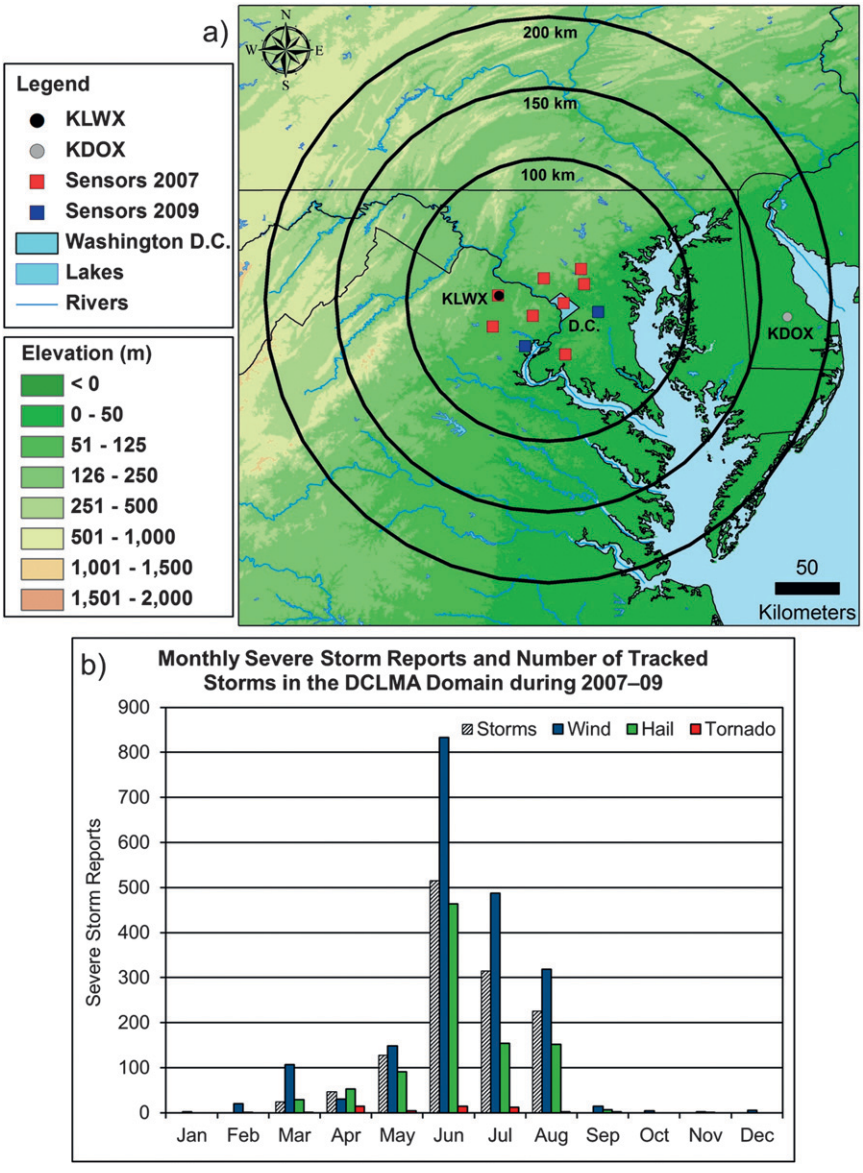

FIG. 1. (a) Overview of the mid-Atlantic study domain. Circles denote the locations of the WSR-88D radars in Dover, DE (gray), and Sterling, VA (black); squares signify the locations of LMA sensors during 2007 (red) and additional sensors added during 2009 (blue); and range rings represent 100-, 150-, and 200-km radii from the center of the DCLMA network (38.95°N, 77.13°W). (b) The total number of severe wind (blue), hail (green), and tornado (red) reports and the number of storms in our dataset within 150 km of the DCLMA during each month (2007–09).

structure, and both LMA and NLDN characteristics to better define relationships between lightning, radar, and storm severity. Based on the assumption that rapidly updating 3D lightning data can provide more timely insights into storm evolution than radar, this study examines ways by which lightning and radar data can complement each other and thereby help provide improved warnings of severe storms. The following sections seek to demonstrate that lightning and radar datasets are complementary, and provide forecasters with context as lightning data and applications become more widely implemented. The study documents interesting relationships between lightning and radar parameters that should motivate future analyses, but does not provide physical explanations for each. The storm analysis techniques and resulting storm database are described first

TABLE 1. Examples of the many lightning and radar parameters that are tracked within individual storms and discussed in this paper.

Abbreviation	Description	Unit
H30above263K	Height of 30-dBZ echo above −10°C	km
H50above273K	Height of 50-dBZ echo above 0°C	km
MESH	Max expected size of hail	mm
Rain rate	Avg rain rate	$mm\,h^{-1}$
LayerAvgRef	Avg reflectivity between 0° and −20°C	dBZ
Top30dBZ	Max height of 30-dBZ echo	km
VIL	Vertically integrated liquid	$kg\,m^{-2}$
Divergence	Storm-top divergence (above 10 km)	s^{-1}
Size	Storm size	km^2
totalLMA	Total LMA flash rate	$Flashes\,min^{-1}$
LMA–FED	LMA flash extent density	$Flashes\,km^{-2}\,min^{-1}$
LMA–FID	LMA flash initiation density	$Flashes\,km^{-2}\,min^{-1}$
VILMA	Vertically Integrated LMA	$Sources\,km^{-2}\,min^{-1}$
HtMaxLMA	Height of max LMA	km
totalCG	Total CG flash rate	$Flashes\,min^{-1}$
cgdensneg	−CG flash density	$Flashes\,km^{-2}\,min^{-1}$
cgmultneg	−CG multiplicity	Strokes
cgpeakneg	−CG estimated peak current (I_p)	kA
Perpos	Percentage of CG flashes that are +CG	%

(section 2). Section 3a then investigates serial correlation in the dataset and documents the persistence of lightning and radar parameters. Finally, section 3b examines the distribution of lightning jumps in severe and nonsevere storms, illustrates differences between severe storm categories (nonsevere, severe wind only, hail only, wind plus hail, and tornadic), and quantifies relationships between lightning and radar parameters.

2. Data and methods

a. Radar and lightning grids

We used a variety of data sources and two software packages to examine the lightning and radar characteristics (Table 1) of many individual storms. Data sources included Weather Surveillance Radar–1988 Doppler (WSR-88D) data, Rapid Update Cycle (RUC) hourly analyses (Benjamin et al. 2004), NLDN-reported CG lightning characteristics, total lightning information from the DCLMA (Krehbiel 2008), and quality-controlled severe weather reports from the NOAA National Climatic Data Center's (NCDC) *Storm Data* publication.

The aforementioned data sources were merged using WDSS-II (Lakshmanan et al. 2006). WDSS-II contains algorithms that extract near-storm environmental variables from hourly RUC analyses, compute reflectivity and velocity parameters from single or multiple WSR-88Ds, and ingest lightning data from the NLDN and LMA networks. We computed many 3D radar parameters by merging data (Lakshmanan et al. 2006) from the WSR-88Ds in Sterling, Virginia, and Dover, Delaware (Fig. 1a), with near-storm environmental information from hourly 20-km RUC analyses (Benjamin et al. 2004). Although RUC analyses do not perfectly represent true atmospheric conditions, they do provide better spatial and temporal resolution than radiosonde soundings.

Rapidly updating radar grids (2-min intervals) were created in WDSS-II using interpolation techniques and the most recent elevation scans from each radar (Lakshmanan et al. 2006). Several studies have examined the use of interpolation techniques to create 3D multiradar grids (e.g., Trapp and Doswell 2000; Askelson et al. 2000; Zhang et al. 2005; Lakshmanan et al. 2006). Lakshmanan et al. (2006) summarized this previous work and demonstrated that their intelligent formulation (implemented in WDSS-II) accounts for the lack of time synchronization between radars, inaccurate time stamps on radar data, varying radar beam geometry with range, vertical gaps between radar scans, storm movement, differing radar calibrations, and beam blockage due to terrain. The present study uses the default exponential weighting function objective analysis scheme implemented in WDSS-II (Zhang et al. 2005; Lakshmanan et al. 2006), and both radars are required to be scanning using the same volume coverage pattern (VCP). Merged radar parameters (Table 1) were computed on a 1 km × 1 km × 1 km grid with 20 vertical levels.

Existing WDSS-II algorithms ingested the NLDN data and created CG flash densities at user-specified spatial and temporal resolutions. We also combined and modified existing WDSS-II algorithms to create grids of positive CG (+CG) percentage, as well as +CG and negative CG (−CG) multiplicity (return strokes) and estimated peak current (I_p, kA). Although the NLDN-derived CG grids were created at 2-min intervals, each 2 km × 2 km grid cell recorded the most recent 10 min of CG flashes to increase the number of flashes used to compute statistics (e.g., average multiplicity). Conversely, we used only 2 min of LMA observations to compute 2 km × 2 km LMA grids every 2 min. This temporal inconsistency limits our ability to directly compare the CG and LMA parameters (e.g., IC/CG ratio). Many questions remain concerning the occurrence and distribution of weak +CG reports (Biagi et al. 2007; Cummins and Murphy 2009; Rudlosky and Fuelberg 2010, 2011).

Cummins and Murphy (2009) suggested that +CG discharges with estimated peak current less than 20 kA are a mixture of CG and IC pulses. Based on findings by Biagi et al. (2007), we removed weak +CG reports with estimated peak current less than 15 kA.

WDSS-II contains algorithms that ingest LMA data and create both source- and flash-based products. LMA networks report the 3D locations of VHF radiation "sources" that are emitted as lightning channels accelerate (Rison et al. 1999). Source-based LMA products that we calculated include the column density of LMA sources (VILMA), the maximum LMA source density at any 1-km level (MaxLMA), and the height at which the MaxLMA occurs (HtMaxLMA). Most previous studies have examined LMA flash distributions rather than source-based LMA products (e.g., Williams et al. 1999; Goodman et al. 2005; MacGorman et al. 2008). A WDSS-II algorithm described by MacGorman et al. (2008) was used to consolidate individual LMA sources into flashes based on spatial and temporal criteria. Previous studies differ on the number of sources required to define an LMA flash [ranging from 1 to 10 sources; e.g., Williams et al. (1999); Lang et al. (2004); Schultz et al. (2009)]. We used the default settings in which the flash consolidation distance thresholds vary with range from the LMA center, but specified that all flashes must contain at least 3 individual LMA sources (instead of the default 10 sources) to account for the lower detection efficiency of the DCLMA (versus the Oklahoma LMA). Only sources detected by at least six sensors were included in the dataset to limit contamination by radio frequency (RF) noise. Flash-based LMA products [e.g., flash extent density (FED), flash initiation density (FID), and flash rate] were computed on a 2 km × 2 km grid with 1-km vertical resolution. Since detection efficiency decreases with range from the network's center, this study only examines storms entirely within 150 km of the DCLMA center (38.95°N, 77.13°W; Fig. 1a). No attempt was made to link the LMA and NLDN flashes, so the LMA parameters described herein count both IC flashes and the upper portions of CG flashes.

b. Data mining storm attributes

Lightning and radar parameters were examined within individual storms using a WDSS-II algorithm (w2segmotion) that identifies and tracks radar- or LMA-defined storm features (Lakshmanan et al. 2009) and extracts information from other gridded fields (Lakshmanan and Smith 2009). The algorithm is a modification of a common image processing technique (watershed transform; Najman and Schmitt 1996) that identifies local maxima and their regions of support (foothills) based on user-defined thresholds (Lakshmanan et al. 2009). We automated w2segmotion to track individual storm areas and output their lightning and radar characteristics to a database at 2-min intervals. The algorithm allowed us to select the field to be tracked (lightning or radar parameters), define the minimum size of features, and set thresholds to facilitate consistent tracking of coherent features.

Lakshmanan et al. (2009) described the w2segmotion thresholds that are required to identify and track storm features. We tracked storms based on their reflectivity at −20°C (Ref20C) since that choice appeared to best isolate discrete storms. The same thresholds were used for all 61 case study days. We specified a maximum Ref20C of 62.5 dBZ, a minimum of 25 dBZ, an increment of 12.5 dBZ, a maximum range (depth) of 37.5 dBZ, and a minimum size (saliency) of 100 km^2. The w2segmotion algorithm first searches for one or more maxima in the defined field (Ref20C). A maximum is defined if its area-averaged Ref20C exceeds 62.5 dBZ. The threshold is then decreased by one increment (12.5 dBZ) to 50 dBZ, and the algorithm again searches for maxima, continuing the incremental search down to a minimum of 25 dBZ.

The algorithm then searches for a region surrounding each maximum that meets the minimum size (saliency) criterion of 100 km^2 and exceeds the new threshold of area averaged Ref20C (i.e., maximum reflectivity minus 12.5 dBZ). If a supporting region is not identified for a particular maximum, the threshold is decreased an additional increment to search for a supporting region. If necessary, this search continues down to a maximum depth (range of Ref20C) of 37.5 dBZ. Each maximum must be surrounded by a supporting region to be identified and tracked by w2segmotion.

WDSS-II computes user-defined lightning and radar characteristics for each trackable storm feature, producing a database at 2-min intervals for all storms that occur on a selected day. Several operators (e.g., *average* and *maximum*) were used to extract gridded information for each storm and time, producing many variations of the lightning and radar parameters. For each storm and time, we calculated both the *average* of all 2 km × 2 km pixels within the storm's tracking boundaries as well as the *maximum* value in any 2 km × 2 km pixel. Although w2segmotion attempts to assign a unique storm identifier to each coherently tracked feature throughout its entirety (Lakshmanan et al. 2009), splits and mergers complicate this process. Therefore, we manually inspected each storm to determine if WDSS-II had assigned different identifiers to what appeared to be the same feature at different times during the tracking period. If so, we consolidated the data points from the different identifiers into a single storm file. Each

TABLE 2. Columns display the number of storms and storm centroid points that occur within 150 km of the DCLMA center, as well as the total and average durations (±standard errors) for all storms and each category of storm severity. The duration (h) is equal to the number of 2-min storm points multiplied by 2 min and divided by 60 min.

Category	Storm count	Storm points	Total duration (h)	Avg duration (min)
All	1252	36 248	1208.3	57.9 ±1.38
Nonsevere	868	18 878	629.3	43.5 ±1.11
Severe	384	17 370	579.0	90.5 ±3.16
Wind	163	6169	205.6	75.7 ±4.29
Hail	77	2933	97.8	76.2 ±6.08
Wind + hail	131	7326	244.2	111.9 ±5.71
Tornado	13	942	31.4	144.9 ±18.34

storm was required to contain at least seven 2-min samples.

The resulting storm database then was inspected using GIS. We first displayed all 2-min storm centroid points and selected storms of interest based on their duration, path, and distance from the radar and DCLMA sensors. Locations of severe weather reports from *Storm Data* were then overlaid on the storm centroids to determine each storm's severity (severe versus nonsevere based on the NWS criteria). The severe designation is applied to the lifetime of the storm, regardless of the timing of the severe weather report. Although this approach helps limit the influence of timing uncertainties in the storm reports, it also decreases differences between the severe and nonsevere distributions of lightning and radar characteristics. Severe storms were further subdivided into severe wind only, severe hail only, severe wind plus hail, and tornadic (with or without wind/hail). Several studies have described errors and uncertainties in the *Storm Data* publication (e.g., Witt et al. 1998; Williams et al. 1999; Trapp et al. 2006), but it remains the most accessible and accurate means for locating and classifying severe storms (Schultz et al. 2009). Despite our careful examination of storm reports using GIS, reporting errors may contribute some ambiguity to our storm severity categories. The final storm database included 868 nonsevere and 384 severe storms (Table 2), 163 (77) produced only severe wind (hail), 131 produced severe wind plus hail, and 13 produced tornadoes.

3. Results and discussion

a. Serial correlation in consecutive storm samples

It is important to examine the influence of our sampling interval on the statistical distributions of lightning and radar characteristics. Assuming that each 2-min storm sample is independent of those before and after will exaggerate the statistical significance of any differences in the distributions. Time series of atmospheric variables always have some degree of autocorrelation, also denoted serial correlation (von Storch and Zwiers 1999). Autocorrelation is defined as the correlation of a set of values with itself, thereby measuring the degree of serial dependence in a time series. Autocorrelation can be computed for various lags, with the number of lags being the number of time intervals that the series is shifted before recomputing the correlation. An autocorrelation function represents the autocorrelations for a series of lags. Autocorrelation is relatively large when sampling at short time intervals, such as our consecutive 2-min storm samples. This temporal autocorrelation must be addressed to accurately assess the statistical significance of the lightning and radar distributions.

The present study uses two methods to account for serial correlation: 1) creating a subset of approximately independent samples (von Storch and Zwiers 1999) and 2) computing effective sample sizes (N_e; Leith 1973). We computed effective sample sizes (N_e) for use in calculating means and standard errors, and used subsets of approximately independent samples to compute correlations. Mean values presented herein retain all 2-min storm samples, but the standard errors are computed using N_e instead of N. Autocorrelation functions were computed for each storm parameter (and storm severity category) to determine the decorrelation time or number of lags before the correlation decreases to less than $1/e$ (~0.3679; Leith 1973). The decorrelation time represents the time between effectively independent samples and is used to determine the N_e (Leith 1973). Specifically, a decorrelation time of four lags (8 min) suggests that every fourth sample of 2-min data is effectively independent and that $N_e = N/4$.

Autocorrelation functions were computed separately for each parameter within each storm that was sampled a minimum of 30 times (i.e., 60-min duration). Separate decorrelation times (effective sample sizes) also were computed for each storm severity category (nonsevere, wind, hail, wind plus hail, and tornado) and mathematical operator (i.e., *maximum* and *average* storm values). The decorrelation time for each storm severity category is the average of the decorrelation times for all individual storms within that category. Results reveal that decorrelation times vary by parameter, severity, and mathematical operator, but the great majority are between three and six lags, suggesting that consecutive 2-min samples (following a storm) are effectively independent after only 6–12 min.

Although the fine temporal resolution (2 min) of our lightning and radar datasets complicates statistical analyses, it also provides an opportunity to investigate storm

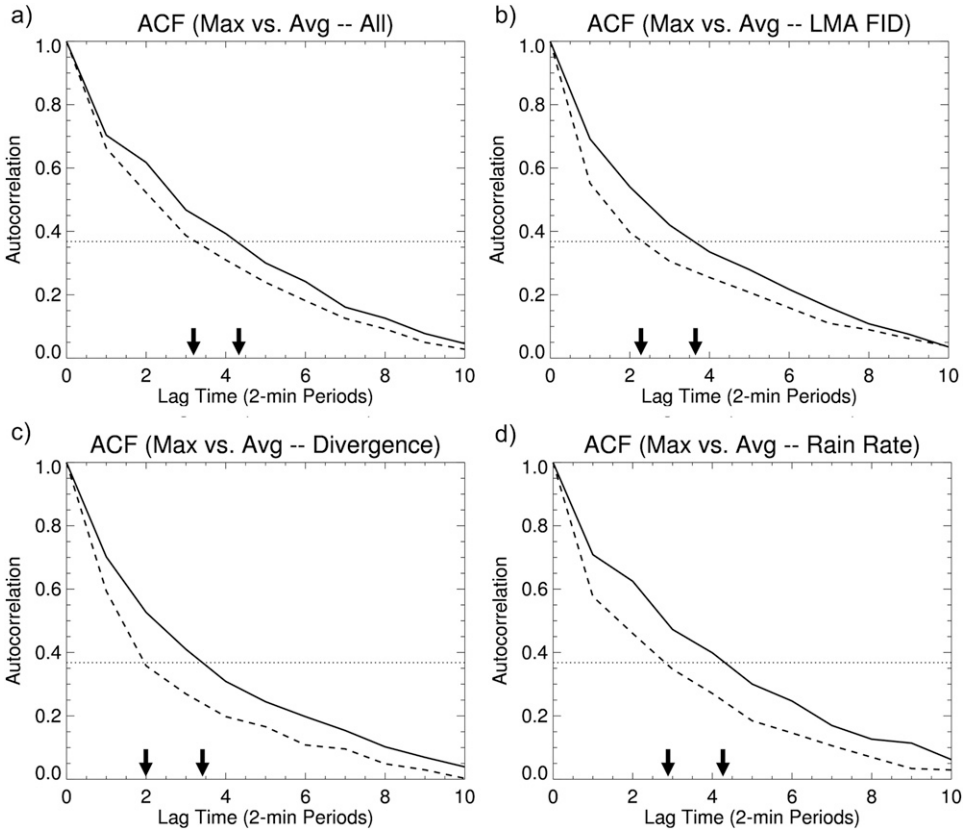

FIG. 2. Autocorrelation functions for *average* storm values (solid) and *maximum* storm values (dashed) for (a) all lightning and radar products listed in Table 1, (b) LMA flash initiation density (LMA–FID), (c) storm-top divergence, and (d) rain rate. Decorrelation times (i.e., when the autocorrelation drops below $1/e$; horizontal dashed lines) are marked with arrows on the horizontal axis. Results show that *average* storm values (solid) are more persistent than *maximum* storm values (dashed).

persistence. Specifically, the decorrelation time can be considered a persistence time scale (von Storch and Zwiers 1999). For time series of different variables with common time increments, relative decorrelation times are useful for comparing system ''memory'' (von Storch and Zwiers 1999). Thus, these statistical methods allow quantitative comparisons of the persistence of individual lightning and radar parameters, as well as the variation of persistence between the different storm severity categories and mathematical operators. Figure 2 shows that *average* storm values (solid) are more persistent than *maximum* values (dashed) for the composite of all lightning and radar parameters listed in Table 1 (Fig. 2a), LMA flash initiation density (LMA–FID; Fig. 2b), storm-top divergence (Fig. 2c), and rain rate (Fig. 2d). This finding is expected since the *maximum* value in a storm can be located at a different 2 km × 2 km pixel every 2 min, while the *average* value is based on all 2 km × 2 km pixels in a storm every 2 min.

Figures 3 and 4 illustrate differences between severe and nonsevere storms and source-based versus flash-based LMA products. Lightning and radar parameters are more persistent in severe storms than nonsevere storms (Fig. 3). The decorrelation time for the maximum expected size of hail (MESH) is approximately three lags (6 min) in nonsevere storms (Fig. 3c) compared to more than six lags (12 min) in tornadic storms (Fig. 3a). A similar relationship exists for LMA flash extent density (LMA–FED), which is effectively independent every six lags (12 min) in storms producing severe wind plus hail (Fig. 3b) versus every three lags (6 min) in nonsevere storms (Fig. 3d). Figure 4a reveals that source-based LMA products (e.g., VILMA) are more persistent than flash-based LMA products (i.e., LMA–FID and LMA–FED) in severe wind plus hail storms. This relationship only exists between LMA–FID and VILMA in nonsevere storms (Fig. 4b), which will require further investigation. The greater persistence of source-based LMA products supports the use of flash-based LMA products for identifying severe storms based on lightning jumps (as done by Schultz et al. 2009, 2011). Specifically, rapid changes may be more easily identified in time series of flash-based

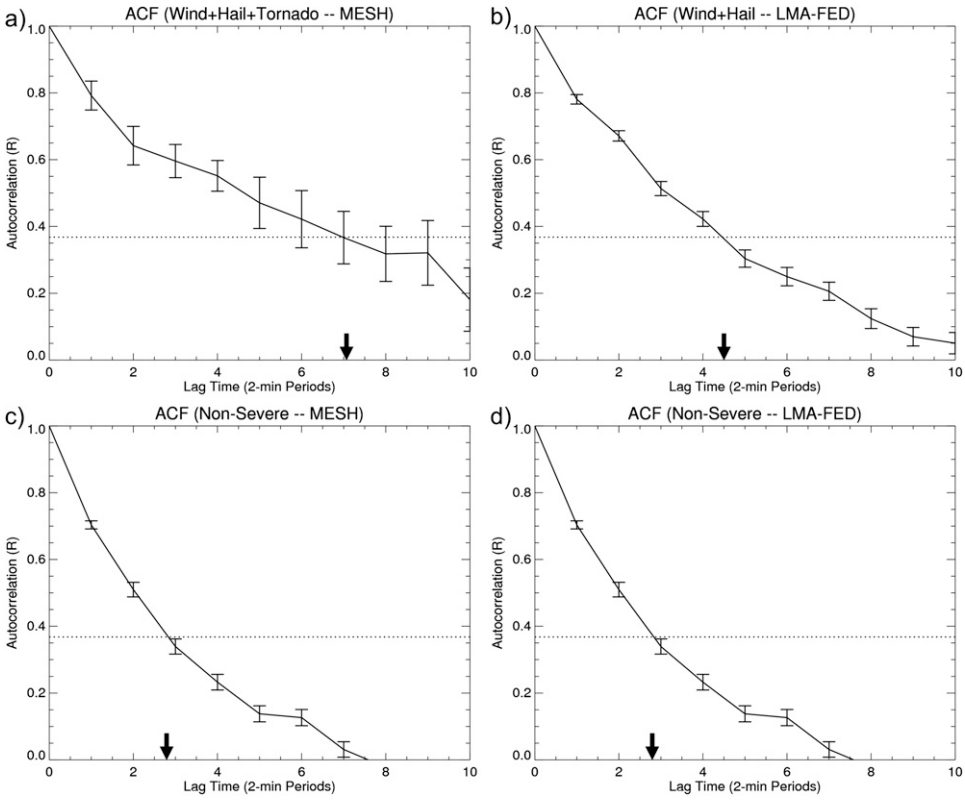

FIG. 3. Autocorrelation functions (with standard errors) for the maximum expected size of hail (MESH) in (a) tornadic and (c) nonsevere storms; and (b),(d) likewise for LMA flash extent density (LMA–FED). Note that lightning and radar parameters are more persistent in severe storms than nonsevere storms.

LMA products than in time series of the seemingly ''smoother'' source-based LMA products.

b. Severe and nonsevere storms

Lightning characteristics are now examined alongside traditional radar-derived measures of storm intensity in severe and nonsevere storms. Recall that a severe storm is defined as any storm that was severe at some time during its life span (as determined by *Storm Data* reports). This approach may introduce errors if a storm is only severe for a small portion of its lifetime. Since nonsevere periods are included in the severe class for long-lived storms, this approach decreases differences between the severe and nonsevere distributions of lightning and radar characteristics. Nonetheless, the approach does help limit the influence of timing uncertainties in the *Storm Data* reports. The following discussion documents many interesting observations, but does not provide physical explanations for each. Rather the findings are presented to motivate future research. Furthermore, our study only documents storms in one geographical region, so it will be important to confirm these observations outside the mid-Atlantic region.

Table 2 documents the distribution of the 1252 storms (36 248 2-min storm samples) in our database that occur entirely within 150 km of the DCLMA center (38.95°N, 77.13°W). Most of our storms occur during June, July, and August (Fig. 1b). The average duration of the ''All'' storms category is approximately 1 h (57.9 min; Table 2), meaning that the database contains more than 1200 h of lightning and radar time series. The dataset includes more than twice as many nonsevere storms (868 nonsevere versus 384 severe), but severe storms (90.5 min) last approximately twice as long as nonsevere storms (43.5 min), so the total periods of data for each are comparable (severe = 579.0 h, nonsevere = 629.3 h).

Recall that the lightning and radar distributions are influenced by the WDSS-II operator used to compute them (i.e., *average* versus *maximum* storm values). Although both columns in Table 3 represent means of all 36 248 storm samples, the *average* column is based on all pixels in a storm at 2-min intervals; whereas the *maximum* column only considers the maximum individual pixel every 2 min. Results indicate that the *average* values are more representative of previously published climatological values than the *maximum* values. For

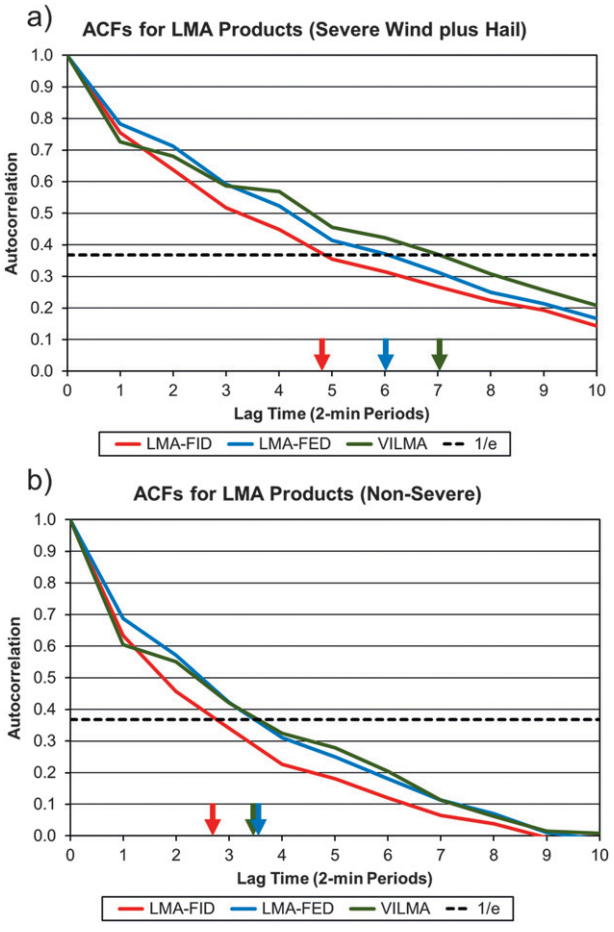

FIG. 4. Autocorrelation functions for LMA flash initiation density (LMA–FID; red), LMA flash extent density (LMA–FED; blue), and vertically integrated LMA (VILMA; green) for (a) severe wind plus hail storms and (b) nonsevere storms. Note that the source-based LMA product (i.e., VILMA) is more persistent than flash-based LMA products (FID and FED).

example, the *average* −CG multiplicity (2.63; Table 3) and estimated peak current (−17.3 kA) are more similar to the climatology of the northeast United States (2.43 and −16.9 kA; Rudlosky and Fuelberg 2010) than are the *maximum* values (4.57 and −27.6 kA). Furthermore, the *average* rain rate (19.3 mm h^{-1}) is more representative of rainfall from entire storm areas than is the *maximum* rain rate (90.2 mm h^{-1}), which only characterizes the maximum 2 km × 2 km pixel in each storm.[2] Nonetheless, since we are interested in storm severity (i.e., when and where storms are most intense), the remainder of this section examines *maximum* values, with the exception of lightning flash rates (flashes min^{-1}) and +CG percentage.

[2] Note that the rain-rate estimates are likely contaminated by hail, and that our study predates the ongoing dual-polarization WSR-88D upgrade that will help address this issue.

TABLE 3. Each column represents a mean (±standard errors) of all 36 248 storm points, but the *average* column characterizes all pixels in a storm every 2 min, whereas the *maximum* column only considers the value of the maximum individual pixel in a storm every 2 min. Note that estimated peak current is abbreviated I_p, max reflectivity refers to the maximum grid cell value at any 1-km vertical level, and that the *average* values are more representative of climatology than the *maximum* values.

Parameter	Avg	Max	Units
MESH	4.1 ±0.06	14.3 ±0.24	mm
Rain rate	19.3 ±0.30	90.2 ±0.66	mm h^{-1}
Max reflectivity	41.8 ±0.13	58.1 ±0.10	dB*Z*
H30above263K	2.8 ±0.04	6.2 ±.05	km
Top30dB*Z*	8.0 ±0.05	11.9 ±0.06	km
HtMaxLMA	8.2 ±0.04	11.9 ±0.06	km
LMA–FED	0.37 ±0.01	1.45 ±0.04	Flashes km^{-2} min^{-1}
LMA–FID	0.03 ±0.001	0.35 ±0.01	Flashes km^{-2} min^{-1}
−CG flash density	0.01 ±0001	0.13 ±0.002	Flashes km^{-2} min^{-1}
−CG multiplicity	2.63 ±0.038	4.57 ±0.077	Strokes
−CG I_p	−17.3 ±0.29	−27.6 ±0.49	kA
+CG multiplicity	1.63 ±0.119	1.68 ±0.125	Strokes
+CG I_p	23.7 ±1.18	24.3 ±1.25	kA

Since lightning jump algorithms are the most common operational application of total lightning data, it is important to examine the distribution of jumps in severe and nonsevere storms. Schultz et al. (2009) examined six ways to define the ''jump'' in their lightning jump algorithm, and showed that a 2σ configuration performed best, yielding an 87% POD and a 33% FAR. Schultz et al. (2011) expanded their analysis to 711 storms and found a 79% POD and 36% FAR. Their algorithm also requires at least 10 flashes min^{-1} before activation so that the normal behaviors of nonsevere thunderstorms and nonsevere stages of severe thunderstorms are not misclassified as severe (Schultz et al. 2009).

The 2σ lightning jump algorithm (Schultz et al. 2009) was applied (with and without flash density thresholds) to each storm in our dataset that lasted at least 30 min (331 severe and 521 nonsevere). The 2σ algorithm with no flash density threshold identifies lightning jumps in 76.4% (90.6%) of nonsevere (severe) storms (Table 4). Use of a simple flash rate threshold (10 flashes min^{-1}) reduces the fraction of jumps in nonsevere (severe) storms to 53.7% (83.9%). Severe and nonsevere storms exhibit a total of 812 and 479 lightning jumps, respectively (not shown), and fewer nonsevere storms exhibit more than one lightning jump (22.8%) than severe storms (58.9%; not shown). Since severe storms typically last longer than nonsevere storms, we also examined the number of lightning jumps per hour. The

TABLE 4. The fraction of severe and nonsevere storms that exhibit lightning jumps using the 2σ algorithm described by Schultz et al. (2009, 2011). Results from three algorithm configurations are shown: 1) no flash density threshold, 2) requires at least 10 flashes min^{-1} before activation, and 3) requires at least 10 flashes min^{-1} and maximum expected size of hail (MESH) >10 mm.

	No flash rate threshold	>10 flashes min^{-1}	>10 flashes min^{-1} and MESH > 10 mm
Nonsevere	76.4	53.7	37.2
Severe	90.6	83.9	77.9

2σ algorithm (with a flash density threshold) yields 0.92 jumps h^{-1} for nonsevere storms and 1.44 jumps h^{-1} in severe storms (Table 5). Despite use of a flash rate threshold, the frequency of jumps in nonsevere storms suggests that additional steps should be taken to reduce these false alarms.

Since inclusion of radar-derived measures of storm intensity might improve the performance of the lightning jump algorithm, we next examine lightning and radar characteristics during 2σ lightning jumps. Lightning jumps in severe storms exhibit a greater average change in flash rate with time (DFRDT; 15.9 versus 9.9 flashes min^{-2}), total LMA flash rate (totLMA; 96.7 versus 54.0 flashes min^{-1}), and MESH (22.6 versus 14.8 mm) than lightning jumps in nonsevere storms (Table 6). Although the automated tracking procedures cause changes in storm shape and size that influence flash rate, DFRDT, and lightning jump occurrence, Table 6 shows that the average change in size is only 16.3 ± 1.12 km^2 (13.3 ± 1.35 km^2) during 2σ lightning jumps in severe (nonsevere) storms. Furthermore, very few jumps (<1%) occur concurrently with large shifts in storm size (>10% growth; not shown). This indicates that the automated tracking procedures produce few erroneous jumps.

Figure 5 displays histograms of LMA flash rate (Fig. 5a), DFRDT (Fig. 5b), and MESH (Fig. 5c) during lightning jumps in severe (red) and nonsevere (blue) storms. Less than 15% of lightning jumps in severe storms have LMA flash rates between 10 and 25 flashes min^{-1} (Fig. 5a) compared to more than 35% having rates greater than 85 flashes min^{-1}. The difference is even more pronounced for MESH (Fig. 5c), with <2% (~34%) of lightning jumps in severe storms exhibiting values less than 5 mm (greater than 25 mm). These findings suggest that a simple MESH threshold might reduce the number of lightning jumps in nonsevere storms (i.e., reduce the FAR).

Applying a 10-mm MESH threshold to the 2σ lightning jump algorithm further reduces the fraction of nonsevere storms exhibiting a jump from 53.7% to 37.2% (Table 4), while the fraction of severe storms with jumps only decreases from 83.9% to 77.9%. The MESH threshold also reduces the frequency of jumps in nonsevere from 0.92 to 0.61 jumps h^{-1} (Table 5). Figure 6 shows the cumulative fraction of all lightning jumps that occur in severe (red) and nonsevere (blue) storms based on MESH thresholds. Less than 30% of lightning jumps with MESH less than 5 mm occur in severe storms, whereas more than 60% of lightning jumps with MESH values greater than 5 mm occur in severe storms. Thus, when a jump occurs, the larger the MESH the greater the likelihood the storm is, was, or will become severe. This finding suggests that MESH values might increase forecaster confidence that a particular jump corresponds to impending severe weather, and suggests that future versions of the lightning jump algorithm should consider including radar parameters.

Approximately 15% of severe storms exhibit no lightning jumps (Table 4). Schultz et al. (2011) identified specific environments in which the lightning jump algorithm may need to be altered to enhance its utility (e.g., low flash rate environments). In the future, it may be possible to include near-storm environment information and/or radar-derived parameters to help tune the lightning jump algorithm and improve its performance under differing conditions. For example, severe hail-only storms exhibit fewer lightning jumps per hour (1.16 jumps h^{-1}; Table 5) than severe wind-only (1.38),

TABLE 5. The fraction of storms exhibiting lightning jumps and the average number of lightning jumps per hour in each storm severity category, using the 2σ algorithm with a minimum flash rate threshold of 10 flashes min^{-1} (Schultz et al. 2009, 2011). The third column shows the frequency of jumps using both the LMA (10 flashes min^{-1}) and MESH (>10 mm) thresholds.

	Fraction of storms with 2σ lightning jumps (LMA threshold)	Avg No. of 2σ lightning jumps per hour (LMA threshold)	Avg No. of 2σ lightning jumps per hour (LMA + MESH threshold)
Nonsevere	53.7	0.92	0.61
Severe	83.9	1.44	1.25
Wind only	80.3	1.38	1.07
Hail only	82.5	1.16	0.98
Wind + hail	88.7	1.58	1.47
Tornado	91.7	1.68	1.45

TABLE 6. Mean (±standard errors) change in flash rate with time (DFRDT), LMA flash rate, maximum expected size of hail (MESH), and change in storm size during 2σ lightning jumps that occurred in severe and nonsevere storms.

	DFRDT (flashes min^{-2})	LMA flash rate (flashes min^{-1})	MESH (mm)	Change in size (km^2)
Nonsevere	9.9 ±0.40	54.0 ±1.68	14.8 ±0.30	13.3 ±1.35
Severe	15.9 ±0.57	96.7 ±2.78	22.6 ±0.31	16.3 ±1.12

severe wind plus hail (1.58), and tornadic (1.68) storms. This observation may be related to the fact that lightning rates sometimes decrease during storm intensification, likely during wet hail growth (e.g., Emersic et al. 2011). Improved understanding of relationships between lightning jumps and specific severe weather types may also improve the operational utility of lightning jump algorithms.

Differences between severe and nonsevere storms are next illustrated using mean lightning and radar characteristics (Tables 7–9). Recall that the mean values are based on all 2-min storm samples, but the standard errors are computed using N_e instead of N ($N_e = N/4$; Fig. 2a). Each of the mean comparisons described below were found to be significant using a two-sample t test, with p values much less than 0.01. In addition to lasting longer (Table 2), severe storms are larger than nonsevere storms (420.0 versus 320.7 km^2; Table 7). Severe storms also exhibit stronger radar-derived parameters (Table 7) and greater LMA (Table 8) and −CG flash rates (Table 9) than nonsevere storms. The mean MESH is 9.0 mm greater in severe storms (19.0 mm) than nonsevere storms (10.0 mm; Table 7), and the 30-dBZ echo-top height (Top30dBZ) is 1.7 km higher in severe storms (12.8 versus 11.1 km). Both the LMA flash rate (53.4 flashes min^{-1}; Table 8) and −CG flash rate (23.4 flashes min^{-1}; Table 9) also are greater in severe storms than nonsevere storms (20.0 LMA flashes min^{-1} and 9.8 −CG flashes min^{-1}).

Several additional differences are evident when storms are categorized by the type of severe weather they produce. Hail-only storms exhibit the lowest mean Top30dBZ (11.7 km; Table 7) and both the smallest LMA (25.2 flashes min^{-1}; Table 8) and −CG flash rates (12.1 flashes min^{-1}; Table 9). Despite having similar values of MESH and rain rate, the wind-only storms exhibit greater LMA and CG flash rates and much greater −CG multiplicity and estimated peak current than hail-only storms (Table 9). These findings likely are due in part to the larger average size of the wind-only storms (474.8 km^2) than the hail-only storms (342.0 km^2). Greater LMA flash rates and stronger −CG characteristics in the wind-only storms suggest that more charge is available for producing IC and CG flashes than in the hail-only storms. The severe wind-only and hail-only storms exhibit weaker values of MESH and rain rate than the wind plus hail and tornadic storms. The mean MESH (rain rate) is ~15 mm (~95 mm h^{-1}) in the wind-only and hail-only storms, compared to MESH exceeding 22 mm

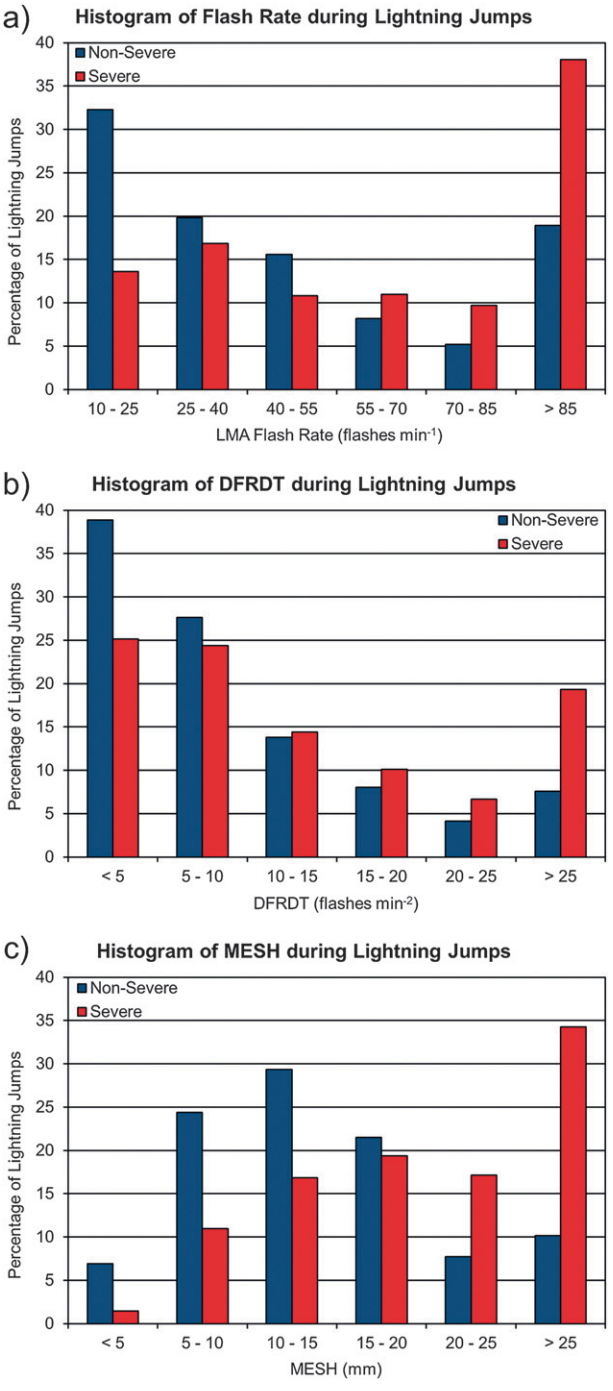

FIG. 5. Histograms of (a) flash rate, (b) change in flash rate with time (DFRDT), and (c) maximum expected size of hail (MESH) during lightning jumps in severe (red) and nonsevere (blue) storms.

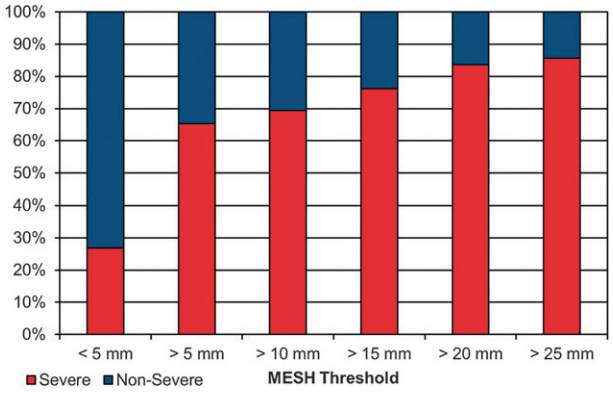

FIG. 6. Fraction of all 2σ lightning jumps that occur in severe (red) and nonsevere (blue) storms based on MESH thresholds (e.g., >5 mm). For example, >60% of lightning jumps with MESH > 5 mm occur in severe storms.

and a rain rate greater than 105 mm h^{-1} in the wind plus hail and tornadic storms (Table 7). Although MESH, rain rate, and Top30dB*Z* are comparable in the wind plus hail and tornadic storms (Table 7), the tornadic storms exhibit much greater LMA (122.6 flashes min^{-1}; Table 8) and −CG flash rates (47.4 flashes min^{-1}; Table 9) than the wind plus hail storms (60.2 LMA flashes min^{-1} and 24.1 −CG flashes min^{-1}). Further research is needed to explain these findings and confirm them outside of our study domain.

Correlation coefficients (Table 10) and profile histograms (Fig. 7) quantify relationships between LMA, NLDN, and radar-derived parameters. Pearson correlation coefficients (*r*; Wilks 2006) were calculated for many pairs of lightning and radar parameters. Recall that subsets of approximately independent samples (i.e., every fourth sample; Fig. 2a) were used to compute correlations. Table 10 contains examples of the many relationships that are significant at the 0.01 level using a two-sample *t* test (Wilks 2006). Although correlations are better between *average* storm values than between *maximum* values (i.e., *r* values generally increase by 0.10–0.25), Table 10 is based on *maximum* storm values for consistency with the preceding discussion. This contributes to the somewhat weak correlations described below. Profile histograms (Fig. 7) are an alternative to scatterplots, and further illustrate relationships between pairs of lightning and radar parameters.

Radar parameters are correlated with both LMA and NLDN characteristics (Table 10). For example, MESH, a composite of several radar parameters, is correlated with both LMA–FED (0.54) and −CG flash density (0.47). WDSS-II estimates MESH by combining radar reflectivity data with Doppler velocities (for rotation and storm-top divergence) and RUC near-storm environment information (to obtain the reflectivity at specific isotherm levels). Thus, MESH responds to both the strength of the updraft and the heights of significant isotherms (e.g., −20°C). Although MESH is greater in severe storms than nonsevere storms (Table 7), Fig. 7a illustrates that LMA–FED increases with increasing MESH regardless of storm severity. This direct relationship between LMA–FED and MESH provides further evidence that LMA flash rates are related to updraft strength (e.g., MacGorman et al. 1989; Steiger et al. 2007; Deierling and Petersen 2008).

Results indicate that flash-based LMA products (e.g., LMA–FED) are better correlated with both CG lightning and radar-derived parameters than are source-based LMA products (e.g., VILMA). For example, LMA–FED is better correlated with both −CG flash density (0.54) and MESH (0.54) than is VILMA (0.28 and 0.26, respectively; not shown). These differences are significant at the 0.01 level based on a Fisher *r*–*z* transformation (Wilks 2006), and suggest that accurate flash counts are essential for determining relationships between LMA, CG, and radar-derived parameters. However, the height of the maximum LMA source density (HtMaxLMA; a source-based product) is correlated with both −CG flash density (0.38) and Top30dB*Z* (0.48; not shown). The mean Top30dB*Z* and HtMaxLMA are both exactly 11.9 (±0.06) km (Tables 7 and 8), providing additional evidence of the relationship between the two.

Since −CG characteristics are indicative of thunderstorm intensity (e.g., Rudlosky and Fuelberg 2011), they

TABLE 7. Mean radar parameters (±standard errors) for all storms and each category of storm severity within 150 km of the LMA center. Other than size, each column represents the *maximum* value in a storm based on 2-min data.

Category	Size (km^2)	MESH (mm)	Rain rate (mm h^{-1})	Top30dB*Z* (km)
All	368.3 ±4.59	14.3 ±0.24	89.9 ±0.66	11.9 ±0.06
Nonsevere	320.7 ±5.57	10.0 ±0.17	81.1 ±0.83	11.1 ±0.05
Severe	420.0 ±7.34	19.0 ±0.39	99.6 ±0.97	12.8 ±0.08
Wind	474.8 ±14.06	15.3 ±0.52	94.1 ±1.47	12.9 ±0.13
Hail	342.0 ±10.54	15.5 ±0.76	95.3 ±2.33	11.7 ±0.17
Wind + hail	390.7 ±11.25	22.7 ±0.83	105.6 ±1.53	13.1 ±0.14
Tornado	531.3 ±14.88	24.4 ±3.57	109.6 ±3.99	13.2 ±0.60

TABLE 8. Mean lightning characteristics (±standard errors) for all storms and each category of storm severity within 150 km of the LMA center. Other than LMA flash rate, each column characterizes the *maximum* value in a storm every 2 min.

Category	LMA flash rate (flashes)	LMA–FED (flashes $km^{-2} min^{-1}$)	LMA–FID (flashes $km^{-2} min^{-1}$)	HtMaxLMA (km)
All	36.0 ±0.64	1.45 ±0.035	0.35 ±0.008	11.9 ±0.06
Nonsevere	20.0 ±0.49	0.98 ±0.027	0.25 ±0.006	11.6 ±0.07
Severe	53.4 ±1.17	1.95 ±0.059	0.45 ±0.013	12.3 ±0.09
Wind	48.3 ±1.34	1.86 ±0.084	0.41 ±0.018	13.0 ±0.14
Hail	25.2 ±1.30	1.22 ±0.109	0.32 ±0.027	11.4 ±0.23
Wind + hail	60.2 ±1.74	2.19 ±0.121	0.51 ±0.027	12.1 ±0.15
Tornado	122.6 ±12.50	3.05 ±0.662	0.63 ±0.121	12.7 ±0.66

also may provide important information about the evolution and severity of storms. Results show that −CG flash density is correlated with Top30dB*Z* (0.65; Table 10) and H30above263K (0.64). Figure 7b reveals that the frequency of −CG flashes increases with increasing storm depth (H30above263K) in both severe and nonsevere storms. Furthermore, Fig. 7c shows that increasing −CG flash densities correspond to increasing LMA–FED in both severe and nonsevere storms. Previous studies have shown that −CG multiplicity and estimated peak current are correlated on both the seasonal and regional scales (Orville et al. 2002; Rudlosky and Fuelberg 2010), and our analysis reveals that −CG multiplicity and estimated peak current also are correlated on the storm scale (0.49; not shown). Specifically, increasing −CG multiplicity corresponds to increasing (absolute values of) estimated −CG peak current. Thus, large multiplicity −CG flashes are most likely to exhibit the strong estimated −CG peak current. Figure 7d shows that this relationship exists in both severe and nonsevere storms, and is very similar between the two groups.

The +CG results suggest that additional caution is needed to account for misclassified weak +CG reports. Weak +CG reports (estimated peak current <15 kA) were omitted from the database because they actually may be misclassified IC flashes (Biagi et al. 2007). Nonetheless, estimated +CG peak current is inversely correlated with various measures of storm intensity (Table 10). Specifically, estimated +CG peak current exhibits weak negative correlations with radar-derived parameters (e.g., Top30dB*Z*; −0.28) and both LMA–FED and −CG flash density (−0.22 and −0.27, respectively). This suggests that ambiguous +CG reports (15–20 kA) become more common as storms intensify (stronger updrafts and taller storms), and that true +CG flashes (>20 kA) are more common in less intense storms. These findings illustrate the complexities of interpreting waveforms from +CG flashes and the influence of both NLDN measurement capabilities and meteorological variability on their relative frequency and distribution (e.g., Rudlosky and Fuelberg 2010, 2011). The inverse relationship between estimated +CG peak current and storm intensity suggests that additional quality control measures beyond the customary weak +CG threshold will be required to accurately document storm-scale +CG distributions in this region.

4. Summary and conclusions

More than 1200 severe and nonsevere storms in the mid-Atlantic region of the United States have been examined using total lightning, radar, and model-derived information. Automated Warning Decision Support

TABLE 9. Mean CG characteristics (±standard errors) for all storms and each storm severity category within 150 km of the LMA center. Other than CG flash rate, each column characterizes the *maximum* value in a storm every 2 min.

Category	CG flash rate (flashes)	−CG density (flashes $km^{-2} min^{-1}$)	−CG multiplicity (strokes)	−CG estimated peak current (kA)	+CG percentage (%)
All	16.3 ±0.26	0.13 ±0.002	4.57 ±0.08	−27.6 ±0.49	3.3 ±0.32
Nonsevere	9.8 ±0.21	0.10 ±0.002	4.04 ±0.08	−26.5 ±0.56	3.5 ±0.36
Severe	23.4 ±0.48	0.16 ±0.004	5.01 ±0.11	−28.5 ±0.65	3.0 ±0.41
Wind	24.3 ±0.69	0.17 ±0.006	5.43 ±0.18	−32.4 ±1.18	2.9 ±0.57
Hail	12.1 ±0.56	0.12 ±0.007	4.04 ±0.25	−23.9 ±1.52	3.9 ±1.44
Wind + hail	24.1 ±0.69	0.17 ±0.007	4.95 ±0.20	−26.7 ±1.10	2.7 ±0.74
Tornado	47.4 ±4.54	0.18 ±0.026	5.37 ±0.84	−28.7 ±5.08	3.4 ±3.14

TABLE 10. Examples of Pearson correlation coefficients (r) between LMA, NLDN, and radar-derived parameters. Correlations were derived only from points within 150 km of the LMA center. These correlations are based on *maximum* values in each storm every 2 min (vs *average* values), and only include every fourth sample to account for serial correlation in the consecutive storm samples. Note that estimated peak current is abbreviated I_p, and that all relationships shown are significant at the 0.01 level.

	LMA–FED	−CG density	+CG I_p
LMA–FED	—	0.54	−0.22
−CG density	0.54	—	−0.27
+CG I_p	−0.22	−0.27	—
H30above263	0.51	0.64	−0.25
H50above273	0.54	0.51	−0.14
MESH	0.54	0.47	−0.15
Rain rate	0.41	0.45	−0.11
LayerAvgRef	0.42	0.43	−0.18
Top30dBZ	0.52	0.65	−0.28
VIL	0.59	0.61	−0.22

System (WDSS) procedures were developed to create grids of lightning and radar parameters, cluster individual storm features, and data mine lightning and radar attributes from many storms. The study first examined the influence of serial correlation, described how autocorrelation functions help account for serial correlation, and used autocorrelation functions to compare the persistence of individual lightning and radar parameters (section 3a). Section 3b then documented the distribution of lightning jumps in severe and nonsevere storms, discussed differences between lightning and radar characteristics in various categories of storm severity (nonsevere, severe wind only, hail only, wind plus hail, and tornadic), and quantified relationships between lightning and radar parameters.

Serial correlation complicated the statistical analyses but also provided an opportunity to examine the persistence of storms. Decorrelation times were found to vary by parameter, severity, and mathematical operator (i.e., *average* versus *maximum* storm values). *Average* storm values are more persistent than *maximum* storm values, and both lightning and radar parameters are more persistent in severe storms than nonsevere storms. Another important finding is that source-based Lightning Mapping Array (LMA) products [e.g., vertically integrated LMA (VILMA)] are more persistent than flash-based LMA products. Despite these differences, the vast majority of decorrelation times are between three and six lags, suggesting that consecutive 2-min storm samples (following a storm) are effectively independent after only 6–12 min.

The development and implementation of lightning jump algorithms motivated an analysis of lightning jumps alongside radar-derived parameters in severe and nonsevere storms. Adding a simple flash rate threshold (10 flashes min^{-1}) to the 2σ lightning jump algorithm (Schultz et al. 2009, 2011) reduces the fraction of nonsevere storms exhibiting jumps from 76.4% to 53.6%. The 2σ algorithm (with threshold) yields 0.92 jumps h^{-1} in nonsevere storms and 1.44 jumps h^{-1} in severe storms. Less than 15% of lightning jumps in severe storms exhibit LMA flash rates between 10 and 25 flashes min^{-1}, versus more than 35% having greater than 85 flashes min^{-1}. On average, lightning jumps in severe storms have greater total LMA flash rate (totLMA), change in flash rate with time (DFRDT), and maximum expected size of hail (MESH) than lightning jumps in nonsevere storms. Furthermore, <2% (~34%) of lightning jumps in severe storms exhibit MESH values less than 5 mm (greater than 25 mm). Only ~25% of all lightning jumps with MESH less than 5 mm occur in severe storms, whereas more than 60% of lightning jumps with MESH values greater than 5 mm occur in severe storms. Applying a 10-mm MESH threshold to the 2σ lightning jump algorithm further reduces the fraction of nonsevere storms exhibiting a jump from 53.7% to 37.2%, and decreases the frequency of jumps in nonsevere storms from 0.92 to 0.61 jumps h^{-1}. Results also indicate that the automated WDSS tracking procedures produce very few erroneous jumps.

The storm database provided additional insights into the distribution of lightning and radar characteristics in severe and nonsevere storms. For example, *average* storm values are more representative of climatology than *maximum* storm values. Severe storms are larger, last longer, and produce stronger radar-derived parameters and greater LMA and negative cloud-to-ground (−CG) flash rates than nonsevere storms. Severe wind-only and hail-only storms appear less intense on average than the severe wind plus hail and tornadic storms. Severe hail-only storms exhibit the lowest mean 30-dBZ echo top (Top30dBZ) and the smallest LMA and −CG flash rates. Conversely, severe wind-only storms have greater LMA and −CG flash rates, and much greater −CG multiplicity and estimated peak current than severe hail-only storms. Although most radar parameters are comparable in wind plus hail and tornadic storms, the tornadic storms exhibit much greater LMA and −CG flash rates.

Correlation coefficients and profile histograms demonstrated storm-scale relationships between CG and LMA characteristics, and between lightning and radar parameters. For example, both LMA flash extent density (LMA–FED) and −CG flash density are directly related to the MESH. This finding further illustrates the dependence of lightning occurrence on updraft strength. Flash-based LMA products are better correlated with

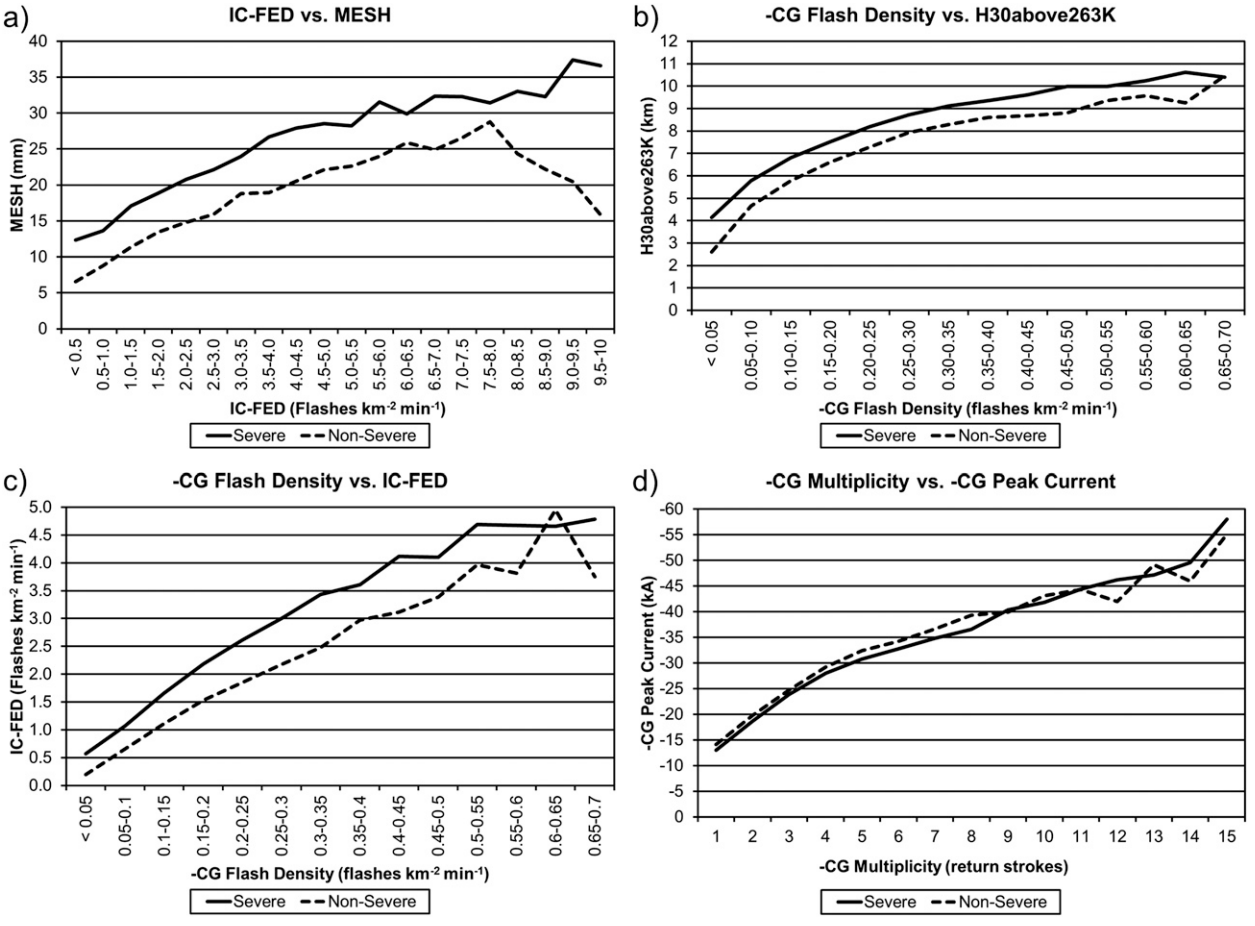

FIG. 7. Profile histograms comparing (a) LMA–FED vs MESH (mm), (b) −CG flash density vs H30above263K (km), (c) −CG flash density vs LMA–FED, and (d) −CG multiplicity (return strokes) vs estimated −CG peak current (kA). The ordinate displays the mean of all values in each corresponding bin, and the solid (dashed) lines represent all 2-min severe (nonsevere) storm centroid points. For example, in (a) the average MESH is 12.5 mm for severe storms with LMA–FID < 0.5 flashes $\mathrm{km}^{-2}\,\mathrm{min}^{-1}$.

CG lightning and radar-derived parameters than are source-based LMA products, indicating that accurate LMA flash counts are required to relate lightning production to storm structure, evolution, and severity. Correlations also were shown between −CG flash density, multiplicity, and estimated peak current; and estimated positive CG (+CG) peak current was found to be inversely related with various lightning and radar-derived measures of storm intensity.

Results suggest that the LMA, NLDN, and radar datasets complement one another, and that their combination might help improve the discernment of storm severity. However, our preliminary findings illustrate complex relationships that will require physical explanations and confirmation outside the mid-Atlantic states. Both the ongoing dual-polarization WSR-88D upgrade and future launch of the Geostationary Operational Environmental Satellite (GOES)-R Geostationary Lightning Mapper (GLM; Goodman et al. 2008) will improve insights into storm-scale processes and the discernment of storm severity. Our future research will continue to examine which combinations of lightning and radar parameters provide clues about the development and evolution of severe storms as we work to incorporate near-storm environment information and radar-derived parameters into operational lightning jump algorithms.

Acknowledgments. Funding for this project was provided by NOAA/NESDIS through the Northern Gulf Institute and the Cooperative Institute for Climate and Satellites as part of the risk reduction activities for the upcoming GOES-R GLM. Vaisala Inc. collected the NLDN data, and the Tallahassee National Weather Service Forecast Office provided them as part of our ongoing collaborations. Additional lightning data were provided by the Washington, D.C., Lightning Mapping Array, which is a joint demonstration project involving NASA, NOAA, and New Mexico Tech. Rapid Update

Cycle model data were obtained from the Atmospheric Radiation Measurement (ARM) program sponsored by the U.S. Department of Energy, Office of Science, Office of Biological and Environmental Research, Climate and Environmental Sciences Division. We thank Valliappa Lakshmanan and Travis Smith for their WDSS-II support, Steve Goodman for his financial support, and Dustin Shea for his many contributions to this project. We also thank three anonymous reviewers for their helpful insights. The contents of this paper are solely the opinions of the authors and do not constitute a statement of policy, decision, or position on behalf of NOAA or the U.S. government.

REFERENCES

Askelson, M. A., J.-P. Aubagnac, and J. M. Straka, 2000: An adaptation of the Barnes filter applied to the objective analysis of radar data. *Mon. Wea. Rev.,* **128,** 3050–3082.

Benjamin, S. G., and Coauthors, 2004: An hourly assimilation–forecast cycle: The RUC. *Mon. Wea. Rev.,* **132,** 495–518.

Betz, H.-D., K. Schmidt, P. Oettinger, and M. Wirz, 2004: Lightning detection with 3-D discrimination of intracloud and cloud-to-ground discharges. *Geophys. Res. Lett.,* **31,** L11108, doi:10.1029/2004GL019821.

Biagi, C. J., K. L. Cummins, K. E. Kehoe, and E. P. Krider, 2007: National Lightning Detection Network (NLDN) performance in southern Arizona, Texas, and Oklahoma in 2003–2004. *J. Geophys. Res.,* **112,** D05208, doi:10.1029/2006JD007341.

Bluestein, H. B., M. M. French, I. PopStefanija, R. T. Bluth, and J. B. Knorr, 2010: A mobile, phased-array Doppler radar for the study of severe convective storms. *Bull. Amer. Meteor. Soc.,* **91,** 579–600.

Boccippio, D. J., S. Heckman, and S. J. Goodman, 2001: A diagnostic analysis of the Kennedy Space Center LDAR network: 1. Data characteristics. *J. Geophys. Res.,* **106,** 4769–4786.

Buechler, D. E., K. T. Driscoll, S. J. Goodman, and H. J. Christian, 2000: Lightning activity within a tornadic thunderstorm observed by the Optical Transient Detector (OTD). *Geophys. Res. Lett.,* **27,** 2253–2256.

Cummins, K. L., and M. J. Murphy, 2009: An overview of lightning locating systems: History, techniques, and data uses, with an in depth look at the U.S. NLDN. *IEEE Trans. Electromagn. Compat.,* **51,** 499–518.

Darden, C. B., D. J. Nadler, B. C. Carcione, R. J. Blakeslee, G. T. Stano, and D. E. Buechler, 2010: Utilizing total lightning information to diagnose convective trends. *Bull. Amer. Meteor. Soc.,* **91,** 167–175.

Deierling, W., and W. A. Petersen, 2008: Total lightning activity as an indicator of updraft characteristics. *J. Geophys. Res.,* **113,** D16210, doi:10.1029/2007JD009598.

Emersic, C., P. L. Heinselman, D. R. MacGorman, and E. C. Bruning, 2011: Lightning activity in a hail-producing storm observed with phased-array radar. *Mon. Wea. Rev.,* **139,** 1809–1825.

Gatlin, P. N., and S. J. Goodman, 2010: A total lightning trending algorithm to identify severe thunderstorms. *J. Atmos. Oceanic Technol.,* **27,** 3–22.

Goodman, S. J., D. E. Buechler, P. D. Wright, and W. D. Rust, 1988: Lightning and precipitation history of a microburst-producing storm. *Geophys. Res. Lett.,* **15** (11), 1185–1188.

——, and Coauthors, 2005: The North Alabama Lightning Mapping Array: Recent severe storm observations and future prospects. *Atmos. Res.,* **76,** 423–437.

——, R. J. Blakeslee, W. Koshak, W. Petersen, D. E. Buechler, P. R. Krehbiel, P. Gatlin, and S. Zubrick, 2008: Pre-launch algorithms and risk reduction in support of the Geostationary Lightning Mapper for GOES-R and beyond. Preprints, *Third Conf. on Meteorological Applications of Lightning Data,* New Orleans, LA, Amer. Meteor. Soc., P3.3. [Available online at https://ams.confex.com/ams/88Annual/webprogram/Paper129401.html.]

Heinselman, P. L., and S. M. Torres, 2011: High-temporal-resolution capabilities of the National Weather Radar Testbed Phased-Array Radar. *J. Appl. Meteor. Climatol.,* **50,** 579–593.

——, D. L. Priegnitz, K. L. Manross, T. M. Smith, and R. W. Adams, 2008: Rapid sampling of severe storms by the National Weather Radar Testbed Phased-Array Radar. *Wea. Forecasting,* **23,** 808–824.

Illingworth, A. J., J. W. F. Goddard, and S. M. Cherry, 1987: Polarization radar studies of precipitation development in convective storms. *Quart. J. Roy. Meteor. Soc.,* **113,** 469–489.

Krehbiel, P. R., 2008: The DC Lightning Mapping Array. Preprints, *Third Conf. on Meteorological Applications of Lightning Data,* New Orleans, LA, Amer. Meteor. Soc., P3.2. [Available online at https://ams.confex.com/ams/88Annual/webprogram/Paper129095.html.]

Lakshmanan, V., and T. Smith, 2009: Data mining storm attributes from spatial grids. *J. Atmos. Oceanic Technol.,* **26,** 2353–2365.

——, ——, K. Hondl, G. J. Stumpf, and A. Witt, 2006: A real-time, three-dimensional, rapidly updating, heterogeneous radar merger technique for reflectivity, velocity, and derived products. *Wea. Forecasting,* **21,** 802–823.

——, ——, G. J. Stumpf, and K. Hondel, 2007: The Warning Decision Support System–Integrated Information (WDSS-II). *Wea. Forecasting,* **22,** 592–608.

——, K. Hondl, and R. Rabin, 2009: An efficient, general-purpose technique for identifying storm cells in geospatial images. *J. Atmos. Oceanic Technol.,* **26,** 523–537.

Lang, T. J., S. A. Rutledge, J. E. Dye, M. Venticinque, P. Laroche, and E. Defer, 2000: Anomalously low negative cloud-to-ground lightning flash rates in intense convective storms observed during STERAO-A. *Mon. Wea. Rev.,* **128,** 160–173.

——, and Coauthors, 2004: The Severe Thunderstorm Electrification and Precipitation Study (STEPS). *Bull. Amer. Meteor. Soc.,* **85,** 1107–1125.

Leith, C. E., 1973: The standard error of time-average estimates of climatic means. *J. Appl. Meteor.,* **12,** 1066–1069.

Loney, M. L., D. S. Zrnic, J. M. Straka, and A. V. Ryzhkov, 2002: Enhanced polarimetric radar signatures above the melting level in a supercell storm. *J. Appl. Meteor.,* **41,** 1179–1194.

MacGorman, D. R., D. W. Burgess, V. Mazur, W. D. Rust, W. L. Taylor, and B. C. Johnson, 1989: Lightning rates relative to tornadic storm evolution on 22 May 1981. *J. Atmos. Sci.,* **46,** 221–251.

——, and Coauthors, 2008: TELEX: The Thunderstorm Electrification and Lightning Experiment. *Bull. Amer. Meteor. Soc.,* **89,** 997–1013.

Najman, L., and M. Schmitt, 1996: Geodesic saliency of watershed contours and hierarchical segmentation. *IEEE Trans. Pattern Anal. Mach. Intell.,* **18,** 1163–1173.

Orville, R. E., 2008: Development of the National Lightning Detection Network. *Bull. Amer. Meteor. Soc.,* **89,** 180–190.

——, G. R. Huffines, W. R. Burrows, R. L. Holle, and K. L. Cummins, 2002: The North American Lightning Detection Network (NALDN)—First results: 1998–2000. *Mon. Wea. Rev.,* **130,** 2098–2109.

Rison, W., R. J. Thomas, P. R. Krehbiel, T. Hamlin, and J. Harlin, 1999: A GPS-based three dimensional lightning mapping system: Initial observations in central New Mexico. *Geophys. Res. Lett.,* **26,** 3573–3576.

Romine, G. S., D. W. Burgess, and R. B. Wilhelmson, 2008: A dual-polarization-radar-based assessment of the 8 May 2003 Oklahoma City area tornadic supercell. *Mon. Wea. Rev.,* **136,** 2849–2870.

Rudlosky, S. D., and H. E. Fuelberg, 2010: Pre- and postupgrade distributions of NLDN reported cloud-to-ground lightning characteristics in the contiguous United States. *Mon. Wea. Rev.,* **138,** 3623–3633.

——, and ——, 2011: Seasonal, regional, and storm-scale variability of cloud-to-ground lightning characteristics in Florida. *Mon. Wea. Rev.,* **139,** 1826–1843.

Ryzhkov, A. V., T. J. Schuur, D. W. Burgess, P. L. Heinselman, S. E. Giangrande, and D. S. Zrnic, 2005: The Joint Polarization Experiment: Polarimetric rainfall measurements and hydrometeor classification. *Bull. Amer. Meteor. Soc.,* **86,** 809–824.

Schultz, C. J., W. A. Petersen, and L. D. Carey, 2009: Preliminary development and evaluation of lightning jump algorithms for the real-time detection of severe weather. *J. Appl. Meteor. Climatol.,* **48,** 2543–2563.

——, ——, and ——, 2011: Lightning and severe weather: A comparison between total and cloud-to-ground lightning trends. *Wea. Forecasting,* **26,** 744–755.

Steiger, S. M., R. E. Orville, and L. D. Carey, 2007: Total lightning signatures of thunderstorm intensity over north Texas. Part I: Supercells. *Mon. Wea. Rev.,* **135,** 3281–3302.

Tessendorf, S. A., K. C. Wiens, and S. A. Rutledge, 2007: Radar and lightning observations of the 3 June 2000 electrically inverted storm from STEPS. *Mon. Wea. Rev.,* **135,** 3665–3681.

Thomas, R. J., P. R. Krehbiel, W. Rison, T. Hamlin, J. Harlin, and D. Shown, 2001: Observations of VHF source powers radiated by lightning. *Geophys. Res. Lett.,* **28,** 143–146.

Trapp, R. J., and C. A. Doswell, 2000: Radar data objective analysis. *J. Atmos. Oceanic Technol.,* **17,** 105–120.

——, D. M. Wheatley, N. T. Atkins, R. W. Przybylinski, and R. Wolf, 2006: Buyer beware: Some words of caution on the use of severe wind reports in postevent assessment and research. *Wea. Forecasting,* **21,** 408–415.

von Storch, H., and F. W. Zwiers, 1999: *Statistical Analysis in Climate Research.* Cambridge University Press, 484 pp.

Weber, M. E., E. R. Williams, M. M. Wolfson, and S. J. Goodman, 1998: An assessment of the operational utility of a GOES lightning mapping sensor. Lincoln Laboratory Project Rep. NOAA-18, 108 pp.

Wiens, K. C., S. A. Rutledge, and S. A. Tessendorf, 2005: The 29 June 2000 supercell observed during steps. Part II: Lightning and charge structure. *J. Atmos. Sci.,* **62,** 4151–4177.

Wilks, D. S., 2006: *Statistical Methods in the Atmospheric Sciences.* 2nd ed. International Geophysics Series, Vol. 91, Academic Press, 648 pp.

Williams, E. R., M. E. Weber, and R. E. Orville, 1989: The relationship between lightning type and convective state of thunderclouds. *J. Geophys. Res.,* **94** (D11), 13 213–13 220.

——, and Coauthors, 1999: The behavior of total lightning activity in severe Florida thunderstorms. *Atmos. Res.,* **51,** 245–265.

Witt, A., M. D. Eilts, G. J. Stumpf, J. T. Johnson, E. D. Mitchell, and K. W. Thomas, 1998: An enhanced hail detection algorithm for the WSR-88D. *Wea. Forecasting,* **13,** 286–303.

Zhang, J., K. Howard, and J. J. Gourley, 2005: Constructing three-dimensional multiple-radar reflectivity mosaics: Examples of convective storms and stratiform rain echoes. *J. Atmos. Oceanic Technol.,* **22,** 30–42.